Fang, X., Park, S., Saito, T., Tunnicliffe, R., Ganesan, A. L., Rigby, M., Li, S., Yokouchi, Y., Fraser, P. J., Harth, C. M., Krummel, P. B., Mühle, J., O'Doherty, S., Salameh, P. K., Simmonds, P. G., Weiss, R. F., Young, D., Lunt, M. F., Manning, A. J., ... Prinn, R. G. (2019). Rapid increase in ozone-depleting chloroform emissions from China. *Nature Geoscience*, *12*(2), 89-93. https://doi.org/10.1038/s41561-018-0278-2

Peer reviewed version

Link to published version (if available):
10.1038/s41561-018-0278-2

Rapid increase in ozone-depleting chloroform emissions from China

Xuekun Fang[1*], Sunyoung Park[2], Takuya Saito[3], Rachel Tunnicliffe[4,5], Anita L. Ganesan[5*], Matthew Rigby[4*], Shanlan Li[2], Yoko Yokouchi[3], Paul J. Fraser[6], Christina M. Harth[7], Paul B. Krummel[6], Jens Mühle[7], Simon O'Doherty[4], Peter K. Salameh[6], Peter G. Simmonds[4], Ray F. Weiss[7], Dickon Young[4], Mark F. Lunt[4], Alistair J. Manning[8], Alicia Gressent[1], Ronald G. Prinn[1]

[1]Center for Global Change Science, Massachusetts Institute of Technology, Cambridge, Massachusetts, USA

[2]Department of Oceanography, Kyungpook National University, Daegu, South Korea

[3]National Institute for Environmental Studies, Tsukuba, Japan

[4]School of Chemistry, University of Bristol, Bristol, UK

[5]School of Geographical Sciences, University of Bristol, Bristol, UK

[6]Climate Science Centre, CSIRO Oceans and Atmosphere, Aspendale, Victoria, Australia

[7]Scripps Institution of Oceanography, University of California, San Diego, La Jolla, California, USA

[8]Met Office, Exeter, United Kingdom

WHEN REVISING YOUR PAPER, PLEASE

* State in a cover note the length of the text, methods and legends; the number of references; number and estimated final size of figures and tables

Length of the text: 2197

Length of the methods: 1392

Number of references: 39

Number of tables: 0

Number of figures: 2

FIRST PARAGRAPH

Chloroform ($CHCl_3$) contributes to the depletion of the stratospheric ozone layer. However, due to its short lifetime and predominantly natural sources, it is not included in the Montreal Protocol that regulates the production and uses of ozone depleting substances. Atmospheric chloroform mole fractions were relatively stable or slowly decreased during 1990-2010. Here, we show that global chloroform mole fractions increased after 2010, based on in situ chloroform measurements at seven stations around the world. We estimate that the global chloroform emissions grew at the rate of 3.5% yr^{-1} between 2010 and 2015 based on atmospheric model simulations. We use two regional inverse modelling approaches, combined with observations from East Asia, to show that emissions from eastern China grew by 49 (41–59) Gg between 2010 and 2015, a change that could explain the entire increase in global emissions. We suggest that if chloroform emissions continuously grow at the current rate, the recovery of the stratospheric ozone layer above Antarctica could be delayed by several years.

Large and effective reductions in emissions of long-lived ozone-depleting substances (ODSs) have been achieved through the 1987 Montreal Protocol and its amendments, evidenced by the observed decline in the atmospheric abundances of many ODSs[1]. Important remaining uncertainties in the timing of ozone layer recovery are due, in part, to the uncertain impact of very short-lived substances (VSLSs), such as dichloromethane (CH_2Cl_2) and chloroform ($CHCl_3$), which are not currently regulated under the Montreal Protocol[1]. Historically, due to the relatively short atmospheric lifetimes (typically <6 months) and therefore low atmospheric concentrations, VSLSs have been thought to play a minor role in stratospheric ozone depletion. However, substantial levels of VSLSs have been detected in the lower stratosphere[2, 3, 4] and numerical model simulations suggest a significant contribution of VSLS to ozone loss in the stratosphere[5, 6, 7]. A recent study shows that CH_2Cl_2 atmospheric concentrations are increasing rapidly and, assuming the concentrations continue to grow, the projected CH_2Cl_2 concentrations could substantially delay the Antarctic ozone layer recovery by nearly 30 years, based on global chemical transport model simulations[8]. This study presents the $CHCl_3$ recent growth, its probable cause and the potential future impact on Antarctic ozone layer recovery.

Atmospheric emissions of $CHCl_3$ are from both natural and anthropogenic sources[9, 10]. Natural sources are dominated by microbial production in the ocean and soil, with minor contributions from volcanic eruptions. Anthropogenic sources are thought to primarily include HCFC-22 ($CHClF_2$) and fluoropolymer production, water chlorination and paper manufacturing[10]. It has generally been believed that atmospheric $CHCl_3$ primarily originates from natural sources (e.g., 90%[9]; mainly ocean and soil processes), with only a small anthropogenic contribution. However, recent studies have suggested that anthropogenic

emissions may have been dramatically under-estimated and that ~50% of $CHCl_3$ emissions may be attributable to these sources[11, 12]. This study also explores the $CHCl_3$ sources and their contributions to recent global $CHCl_3$ changes.

Recent growth in global $CHCl_3$ mole fractions and emissions

Previous studies using Antarctic firn air showed that Southern Hemisphere polar atmospheric mole fractions increased from 3.7 pmol mol^{-1} in 1920 to a peak of 6.5 pmol mol^{-1} in 1990 before decreasing until the end of the record, in 1997[11] (see Figure 1a and b). Based on firn air samples from Arctic and Antarctic sites, Northern Hemisphere mole fractions increased from 5.7 pmol mol^{-1} in 1920, peaked at 17 pmol mol^{-1} in 1990 and decreased after that[12] (Figure 1a and b). There are likely calibration differences between these records, but a general picture of increasing concentrations until 1990 and decreasing concentrations after 1990 emerges from both records. *In situ* baseline measurements (observations with pollution events removed using a statistical filtering algorithm[13]) from the Advanced Global Atmospheric Gases Experiment (AGAGE[13]; see station locations in Figure 1a) show that this downward trend continued until around 2010 at remote sampling locations (Figure 1c). At these AGAGE stations, growth rates between 1995 and 2010 varied between -0.8% yr^{-1} (at American Samoa Observatory in the Southern Hemisphere; SMO) and -0.3% yr^{-1} (at Trinidad Head, California, USA, in the Northern Hemisphere; THD), with the trends observed at other stations (Mace Head, Ireland (MHD); Ragged Point, Barbados (RPB); Cape Grim, Tasmania, Australia (CGO)) lying in between these values. However, we find a renewed growth of global $CHCl_3$ mole fractions between 2010 and 2015. After 2010, baseline $CHCl_3$ mole fractions grew in both hemispheres at a higher rate than has been

observed before in the *in situ* or firn records (Figure 1c). During 2010–2015, growth rates for the five AGAGE stations between 2010 and 2015 varied between 2.6% yr^{-1} at CGO and 6.3% yr^{-1} at THD. The changes in global mean mole fractions (output from model simulations incorporating measurement data from these five stations; see Methods) were -0.7% yr^{-1} during 1995−2010 and increased to 3.9% yr^{-1} during 2010−2015. The growth in $CHCl_3$ mole fractions suggests an increase in global $CHCl_3$ emissions, and the higher rate of increase in the Northern Hemisphere compared to the Southern Hemisphere suggests that the increase in $CHCl_3$ emissions occurred mainly in the Northern Hemisphere. The abundance of $CHCl_3$ in the Northern Hemisphere is around 3 times greater than in the Southern Hemisphere, reflecting that the major sources of $CHCl_3$ are in the Northern Hemisphere.

An atmospheric model has been used to estimate global emissions using $CHCl_3$ mole fraction data from five non-Asian AGAGE stations (see Methods). The global inversion carried out using this model shows that annual global-total $CHCl_3$ emissions approximately stabilized at ~271 Gg yr^{-1}, during 2000−2010, with a suggestion of a small decline, and then an increase after 2010, reaching 324 (261−397) Gg yr^{-1} (16−84 percentiles range) in 2015 (Figure 1c). The average rate of increase in global emissions between 2010 and 2015 was approximately 3.5% yr^{-1}.

Whilst the baseline observations at the five non-Asian AGAGE stations grew between 2010 and 2015, the magnitude of pollution events (i.e. the enhanced mole fractions due to the transport of $CHCl_3$ from nearby emissions sources, with a magnitude defined here as the 90^{th} percentile of measurements in a year minus the 10^{th} percentile) did not grow significantly at these stations over 2007−2015 (Figure S1 and Table S1). This finding indicates that regional $CHCl_3$ emissions in Australia (CGO station), the west coast of North America (THD station)

and Europe (MHD station) likely did not increase in this period. In contrast, measurements from Hateruma, Japan (HAT) and Gosan, South Korea (GSN) (see measurement information in Methods for details), show increasing magnitudes of above-baseline pollution events over 2010−2015 (Figure 2a), which suggests an increase in $CHCl_3$ emissions in eastern Asia, assuming annual mean meteorological conditions have not changed significantly during 2007−2015. Because the observations qualitatively indicate increasing emissions only from eastern Asia, we have focused our analysis on this region in the following sections.

Rapid increase in China's $CHCl_3$ emissions

To quantify $CHCl_3$ emissions from eastern Asia, two three-dimensional atmospheric dispersion models (FLEXible PARTicle dispersion model (FLEXPART)[14] and the UK Met Office's Numerical Atmospheric-dispersion Modelling Environment (NAME)[15]) were used to simulate the transport of $CHCl_3$ from potential sources to the measurement locations. Two different inverse modelling approaches were used with each of these models: a Bayesian inversion was used with FLEXPART, and a hierarchical Bayesian "trans-dimensional" approach with NAME[16]. For convenience, we label the inversions "FLEXPART" and "NAME" after the transport models, but it should be noted that the statistical approach to inferring fluxes is different with each model (see all details in Methods). Observations and simulations of $CHCl_3$ mole fractions at the two East Asian stations from FLEXPART and NAME inversions are shown in Figure S2.

Results from both the FLEXPART and NAME inversions show a rapid increase of $CHCl_3$ emissions from eastern China after around 2010 (Figure 2c). Total $CHCl_3$ emissions from eastern China were stable during 2008−2010, being 38 (33−44) Gg yr^{-1} on average.

After that the emissions increased by more than a factor of 2, reaching 88 (80−95) Gg yr^{-1} (FLEXPART inversion) and 82 (70−101) (NAME inversion) in 2015. $CHCl_3$ emissions in other East Asian countries/regions were not found to have changed substantially since 2007 (Table S2) and were overall much smaller than eastern China's $CHCl_3$ emissions. Japan and South Korea rank second and third in this region, with emissions of around 4.7 Gg yr^{-1} and 1.7 Gg yr^{-1} on average, respectively. Emissions of $CHCl_3$ in North Korea and Taiwan in most years were smaller than 1.0 Gg yr^{-1}. Thus, $CHCl_3$ emissions from eastern China contributed ~87% of East Asian total emissions between 2007 and 2015.

Compared to 2010, 2015 global $CHCl_3$ emissions increased by 46 (30−61) Gg, while emissions from eastern China increased by 48 (42−54) Gg (FLEXPART inversion) and 50 (41−63) Gg (NAME inversion) (Figure 2d). Therefore, eastern China's emission increase is almost equal to the inferred global emission increase. As mentioned above, $CHCl_3$ emissions from Australia, North America and Europe likely did not change substantially during this period. Thus, the post-2010 global $CHCl_3$ emission increase found in this study is most likely due to the rapid emission increase in eastern China, assuming that there are no substantial $CHCl_3$ emission changes in other regions of the world not covered by the AGAGE measurement network.

Between 2007 and 2015, the highest emissions were inferred for the eastern parts of China, which are highly populated and industrialized. The inferred emissions distribution is broadly consistent with the locations (see Table S3) of factories producing $CHCl_3$ (Figure 2b from the FLEXPART inversion and Figure S3 from the NAME inversion). However, the exact process or processes responsible for the emissions cannot be identified in this analysis. Between 2010 and 2015, the inferred spatial distribution of $CHCl_3$ emissions did not change

136 substantially as emissions rose (see Figure S4). These considerations lead us to conclude that
137 it is most likely that anthropogenic sources are responsible for the rapid emission increase in
138 eastern China during 2010−2015. Recent studies have shown that emissions from eastern
139 Asia of several other ODSs have not declined as expected, or have also increased (e.g., CFC-
140 11[17], CCl_4[18, 19], CFC-114 and CFC-115[20]). It is unclear to what extent, if any, the rise in
141 $CHCl_3$ emissions from China is related to these findings.

142 ## Implications for ozone layer recovery

143 The Antarctic ozone 'hole', a seasonal thinning of the ozone layer above Antarctica
144 during spring, has been predicted to return to pre-1980 levels by around 2050 (±5 years)[17] or,
145 in more recent studies, towards the end of the century[18, 19]. These 'return date' studies have
146 generally not considered the impact of recent growing levels of the major VSLS, CH_2Cl_2 and
147 $CHCl_3$. However, a recent study has shown that continued growth of CH_2Cl_2 at current rates
148 could delay Antarctic ozone recovery by several decades[8]. Here, we use the results of this
149 CH_2Cl_2 study to approximate the potential future impact of the increased $CHCl_3$ on ozone
150 recovery (see Methods). This method relies on the similarities of the CH_2Cl_2 and $CHCl_3$
151 lifetime (both 0.4 years[21]) and their atmospheric distribution. We estimate that the increase in
152 $CHCl_3$ since 2010 could delay Antarctic ozone recovery by ~0.4 year if there is no further
153 growth in $CHCl_3$ abundance beyond 2015. If growth continued at the average rate observed
154 between 2010 and 2015, the delay could be 4–8 years. If the total increase since 1920 is
155 considered, rather than the increase since 2010, these calculated delays are 1 year and 5–9
156 years, respectively. Thus, $CHCl_3$ could have an important role in future ozone layer recovery,
157 especially if mole fractions continue to increase as they have between 2010 and 2015.

Recent studies show that the Asian summer/winter monsoon and the summertime typhoons could provide efficient pathways for directly transporting air pollutants in Asia to the upper troposphere and lower stratosphere[e.g., 22, 23, 24, 25, 26, 27]. During the late boreal summer and fall, nearly one-fifth of the air in the tropical lower stratosphere had previous contact with the planetary boundary layer over Asia, while negligible fractions originate from over North America and Europe[28]. Thus, $CHCl_3$ emitted from East Asia is likely more important for ozone depletion than $CHCl_3$ emitted from other regions of the world. Demand for $CHCl_3$ in China is expected to increase in the main application sector - producing polytetrafluoroethylene - at a growth rate of 7%/yr during 2015–2020[29] (see details in SI), which is consistent with our scenario of increasing $CHCl_3$ emissions and mole fractions, at least in the near-term. Considering the above phenomenon of efficient-transport from Asia to the stratosphere and the substantial amount of $CHCl_3$ emitted in China, the increasing $CHCl_3$ emissions from China pose a growing threat to ozone layer recovery.

The spatial distribution of our derived emissions strongly suggests that anthropogenic activities, rather than natural sources, are driving the observed rise in China's $CHCl_3$ emissions. Chloroform and other VSLSs are not controlled by the Montreal Protocol, because, apart from CH_2Cl_2, they were previously thought to be mostly from natural sources and to have a minor impact on stratospheric ozone due to their relatively short atmospheric lifetimes. However, this study reveals growing amounts of $CHCl_3$ from anthropogenic sources in China, with the potential to delay future ozone layer recovery by around 0.4–8 years, depending on whether $CHCl_3$ abundances pause at the 2015 level, or continue growing at their current rate.

References for main text

1. WMO *Scientific Assessment of Ozone Depletion: 2014. Global Ozone Research and Monitoring Project — Report No. 55* http://ozone.unep.org/Assessment_Panels/SAP/Scientific_Assessment_2010/index.shtml (2014)

2. Navarro, M. A.*, et al.* Airborne measurements of organic bromine compounds in the Pacific tropical tropopause layer. *Proc. Natl. Acad. Sci. U.S.A.* **112,** 13789–13793 (2015).

3. Sala, S.*, et al.* Deriving an atmospheric budget of total organic bromine using airborne in situ measurements from the western Pacific area during SHIVA. *Atmos. Chem. Phys.* **14,** 6903-6923 (2014).

4. Laube, J. C.*, et al.* Contribution of very short-lived organic substances to stratospheric chlorine and bromine in the tropics - a case study. *Atmos. Chem. Phys.* **8,** 7325-7334 (2008).

5. Hossaini, R.*, et al.* Efficiency of short-lived halogens at influencing climate through depletion of stratospheric ozone. *Nat. Geosci.* **8,** 186-190 (2015).

6. Sinnhuber, B. M., Meul, S. Simulating the impact of emissions of brominated very short lived substances on past stratospheric ozone trends. *Geophys. Res. Lett.* **42,** 2449-2456 (2015).

7. Salawitch, R. J.*, et al.* Sensitivity of ozone to bromine in the lower stratosphere. *Geophys. Res. Lett.* **32,** 811-815 (2005).

8. Hossaini, R.*, et al.* The increasing threat to stratospheric ozone from dichloromethane. *Nat. Commun.* **8,** 15962-15970 (2017).

9. McCulloch, A. Chloroform in the environment: occurrence, sources, sinks and effects. *Chemosphere* **50,** 1291-1308 (2003).

10. WMO *Scientific assessment of ozone depletion: 2010. Global Ozone Research and Monitoring Project — Report No. 52* http://ozone.unep.org/Assessment_Panels/SAP/Scientific_Assessment_2010/index.shtml (accessed January 1, 2012) (2011)

11. Trudinger, C. M.*, et al.* Atmospheric histories of halocarbons from analysis of Antarctic firn air: Methyl bromide, methyl chloride, chloroform, and dichloromethane. *J. Geophys. Res. Atmos.* **109,** 310-324 (2004).

12. Worton, D. R.*, et al.* 20th century trends and budget implications of chloroform and related tri-and dihalomethanes inferred from firn air. *Atmos. Chem. Phys.* **6,** 2847-2863 (2006).

13. Prinn, R. G.*, et al.* History of chemically and radiatively important atmospheric gases from the Advanced Global Atmospheric Gases Experiment (AGAGE). *Earth Syst. Sci. Data* **10,** 985-1018 (2018).

14. Stohl, A., Hittenberger, M., Wotawa, G. Validation of the Lagrangian particle dispersion model FLEXPART against large-scale tracer experiment data. *Atmos. Environ.* **32,** 4245-4264 (1998).

15. Jones, A., Thomson, D., Hort, M., Devenish, B. The U.K. Met Office's Next-Generation Atmospheric Dispersion Model, NAME III. In: Borrego C, Norman A-L (eds). *Air Pollution Modeling and Its Application XVII*. Springer US, 2007, pp 580-589.

16. Ganesan, A. L.*, et al.* Characterization of uncertainties in atmospheric trace gas inversions using hierarchical Bayesian methods. *Atmos. Chem. Phys.* **14,** 3855-3864 (2014).

17. Montzka, S. A.*, et al.* An unexpected and persistent increase in global emissions of ozone-depleting CFC-11. *Nature* **557,** 413-417 (2018).

18. Lunt, M. F.*, et al.* Continued Emissions of the Ozone-Depleting Substance Carbon Tetrachloride From Eastern Asia. *Geophys. Res. Lett.* **0,** (2018).

19. Park, S.*, et al.* Toward resolving the budget discrepancy of ozone-depleting carbon tetrachloride (CCl4): an analysis of top-down emissions from China. *Atmos. Chem. Phys.* **18,** 11729-11738 (2018).

20. Vollmer, M. K.*, et al.* Atmospheric histories and emissions of chlorofluorocarbons CFC-13 (CClF3), ΣCFC-114 (C2Cl2F4), and CFC-115 (C2ClF5). *Atmos. Chem. Phys.* **18,** 979-1002 (2018).

21. WMO *Assessment for Decision-Makers: Scientific Assessment of Ozone Depletion: 2014. Global Ozone Research and Monitoring Project—Report No. 56* (2014)

22. Hossaini, R., *et al.* A multi-model intercomparison of halogenated very short-lived substances (TransCom-VSLS): linking oceanic emissions and tropospheric transport for a reconciled estimate of the stratospheric source gas injection of bromine. *Atmos. Chem. Phys.* **16,** 9163-9187 (2016).

23. Yu, P., *et al.* Efficient transport of tropospheric aerosol into the stratosphere via the Asian summer monsoon anticyclone. *Proc. Natl. Acad. Sci. U.S.A.* **114,** 6972-6977 (2017).

24. Randel, W. J., *et al.* Asian Monsoon Transport of Pollution to the Stratosphere. *Science* **328,** 611-613 (2010).

25. Vogel, B., *et al.* Fast transport from Southeast Asia boundary layer sources to northern Europe: rapid uplift in typhoons and eastward eddy shedding of the Asian monsoon anticyclone. *Atmos. Chem. Phys.* **14,** 12745-12762 (2014).

26. Oram, D. E., *et al.* A growing threat to the ozone layer from short-lived anthropogenic chlorocarbons. *Atmos. Chem. Phys.* **17,** 11929-11941 (2017).

27. Ashfold, M. J., *et al.* Rapid transport of East Asian pollution to the deep tropics. *Atmos. Chem. Phys.* **15,** 3565-3573 (2015).

28. Orbe, C., Waugh, D. W., Newman, P. A. Air-mass origin in the tropical lower stratosphere: The influence of Asian boundary layer air. *Geophys. Res. Lett.* **42,** 4240-4248 (2015).

29. Qianzhan. China's fluoropolymer production capacity will be 230,000 tons by 2020, and PTFE will account for 70% (in Chinese). 2017. Available from: https://www.qianzhan.com/analyst/detail/220/170629-c33a2ca7.html

Acknowledgements

X.F., R.G.P., and A.G. are supported by the National Aeronautics and Space Administration (NASA, USA) grants NAG5-12669, NNX07AE89G, NNX11AF17G and NNX16AC98G to MIT. T.S., Y.Y., and the Hateruma station are supported fully by the Ministry of Environment of Japan and NIES. S.P., S.L., and the Gosan AGAGE station are supported by the Basic Science Research Program through the National Research Foundation of Korea (NRF) funded by the Ministry of Education (No. NRF-2016R1A2B2010663). R.T. was funded under Natural Environment Research Council (NERC) grant NE/M014851/1. A.L.G. was funded under a NERC Independent Research Fellowship NE/L010992/1. M.R. was funded under a NERC Advanced Fellowship NE/I021365/1. P.J.F., P.B.K. and the Cape Grim AGAGE station are supported by CSIRO, the Bureau of Meteorology, Refrigerant Reclaim Australia and MIT. The operation of the AGAGE stations were/are supported by the National Aeronautics and Space Administration (NASA, USA) (grants NAG5-12669, NNX07AE89G, NNX11AF17G and NNX16AC98G to MIT; grants NAG5-4023, NNX07AE87G, NNX07AF09G, NNX11AF15G, NNX11AF16G, NNX16AC96G and NNX16A97G to SIO). Mace Head, Ireland, is supported by the Department for Business, Energy & Industrial Strategy (BEIS, UK, formerly the Department of Energy and Climate Change (DECC)) contract 1028/06/2015 to the University of Bristol and the UK Meteorological Office; Ragged Point, Barbados was/is supported by the National Oceanic and Atmospheric Administration (NOAA, USA), contract RA-133-R15-CN-0008 to the University of Bristol; the National Oceanic and Atmospheric Administration supports the operations of the American Samoa station.

Author contributions

X.F. and R.G.P. were responsible for the overall project design. M.R. contributed to the global emission estimation. X.F. contributed to the FLEXPART-based inversions. A.L.G., R.T., A.M., and M.L. contributed to NAME-based inversions. T.S. and Y.Y. provided the $CHCl_3$ measurement data from HAT, Japan. S.P. and S.L. provided the $CHCl_3$ measurement data from GSN, South Korea. Other co-authors provided the $CHCl_3$ measurement data from the five AGAGE stations and the SIO/NIES calibration scales intercomparison data. The manuscript was written by X.F., M.R., A.L.G., J.M., and P.J.F. with contributions from all co-authors.

Competing financial interests

The authors declare no competing financial interests.

Corresponding author

*e-mail: fangxk@mit.edu (X.F.); anita.ganesan@bristol.ac.uk (A.L.G.); matt.rigby@bristol.ac.uk (M.R.)

Additional information

Supplementary Information is available for this paper at https://doi.org/xxxxxxx.

Reprints and permissions information is available at www.nature.com/reprints.

Publisher's note: Springer Nature remains neutral with regard to jurisdictional claims in published maps and institutional affiliations.

Figures

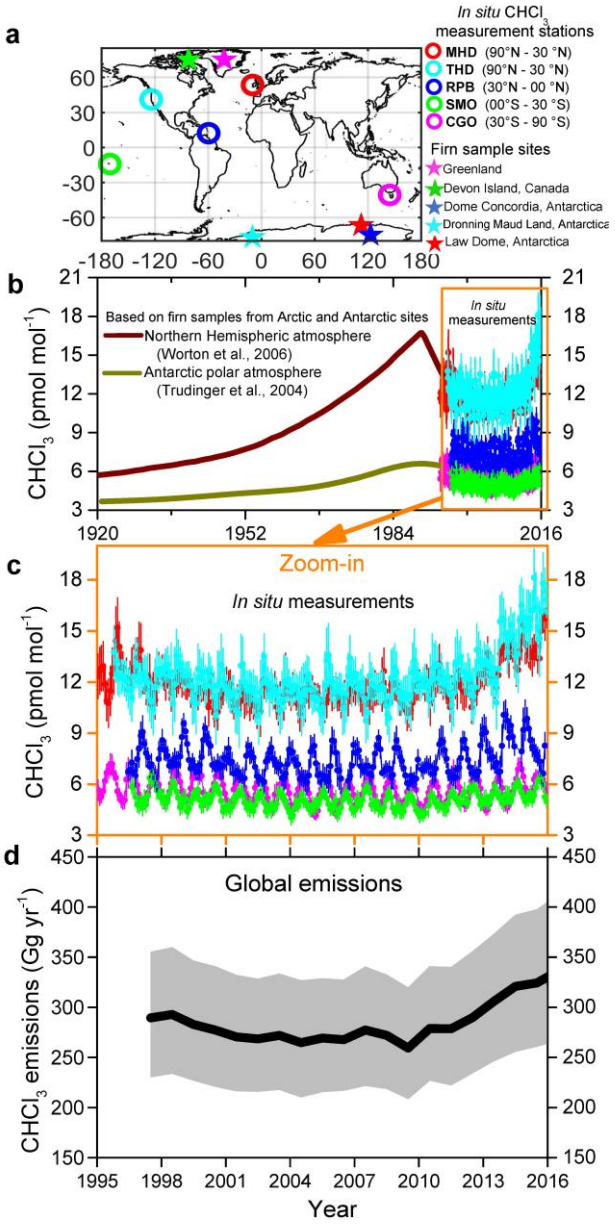

Figure 1. Global atmospheric $CHCl_3$ mole fractions and emissions. **a**, Locations of AGAGE $CHCl_3$ measurement stations used in the global study. **b**, Northern Hemispheric $CHCl_3$ mole fractions, based on $CHCl_3$ mole fractions measured in Arctic and Antarctic firn air[12], and Southern Hemispheric polar $CHCl_3$ mole fractions, based on $CHCl_3$ mole fractions measured in Antarctic firn air[11]; measured $CHCl_3$ mole fractions (baseline data) at the AGAGE stations. **c**, Measured $CHCl_3$ mole fractions at the five remote AGAGE stations during 1995−2015. **d**, Global $CHCl_3$ emissions (black line) and their uncertainties (gray shaded area; 16−84 percentiles) derived from global inverse modeling.

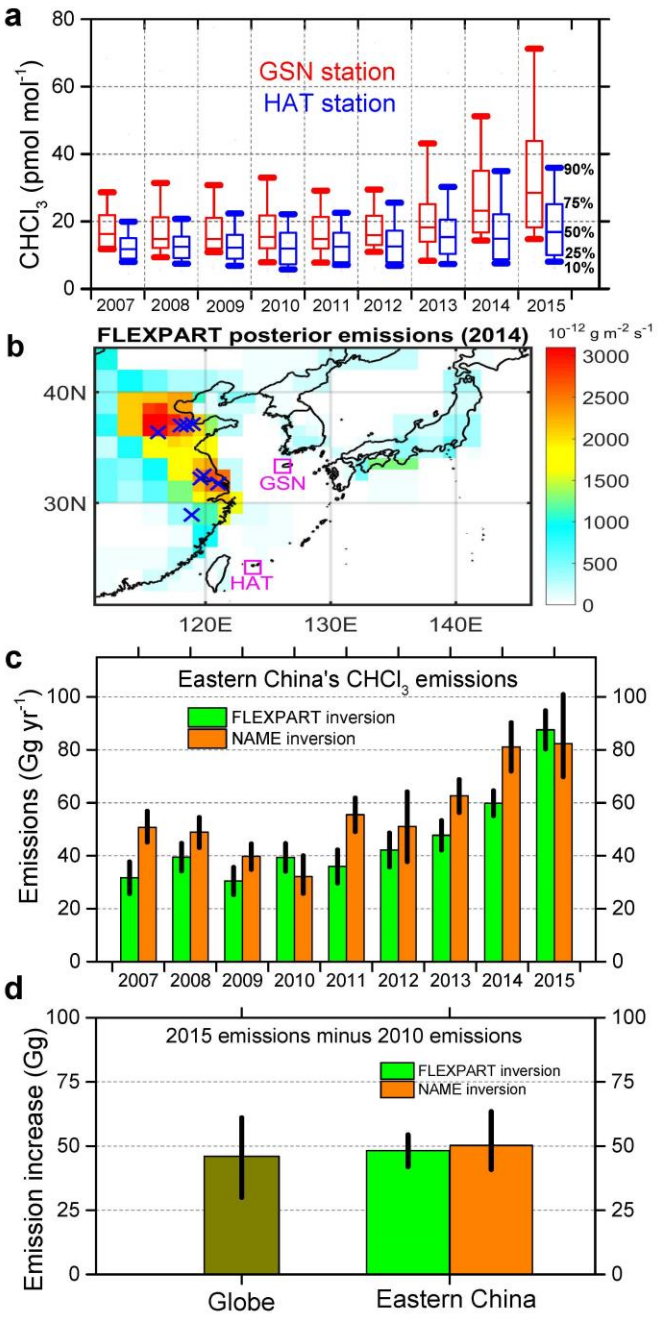

Figure 2. Measured atmospheric $CHCl_3$ mole fractions at Hateruma (HAT) and Gosan (GSN) stations and estimated emissions in eastern China from regional inverse modeling. a, Box and whisker plots of atmospheric $CHCl_3$ mole fractions measured at HAT and GSN stations. **b**, Map of posterior $CHCl_3$ emissions derived from regional inverse modeling using FLEXPART model. The blue crosses represent the factories of $CHCl_3$ production. **c**, Eastern China's yearly total $CHCl_3$ emissions derived from FLEXPART (1**σ** uncertainty) and NAME (5−95 percentile range uncertainty) regional inverse modeling. **d**, 2015 emissions minus 2010 emissions for the total globe and for eastern China.

Methods

$CHCl_3$ measurements and global emissions estimations. Atmospheric mole fractions of $CHCl_3$ are measured at five remote non-Asian AGAGE stations (see information on the five stations in Table S4), using gas chromatography with electron capture detection (GC-ECD) analytical techniques[13]. Global emissions were estimated using baseline mole fractions at the five AGAGE stations and an atmospheric box model[30, 31]. The model separates the atmosphere into four equal-mass zonal bands (90ºN-30°N-0º-30ºS-90ºS), with vertical divisions at 500 hPa and 200 hPa. The inversion used a Bayesian framework in which the rate of change of emissions was constrained by a prior estimate[32]. The prior emissions growth rate was assumed to be zero, with an uncertainty in the emissions growth of ±20% of the global total emissions, based on Xiao et al.[33]. Uncertainties in the derived fluxes include those due to the observations, the prior constraint, and the atmospheric lifetime (following Rigby et al.[34]). More information is provided in Supplementary Information.

$CHCl_3$ measurements and emissions estimation for East Asia. Atmospheric mole fractions of $CHCl_3$ measured at two Asian stations (HAT and GSN, see Figure 2b) were used in an inverse modeling study to derive East Asian emissions. The HAT station (24.1°N, 123.8°E) is located on a small island at the southern edge of the Japanese archipelago and to the east of Taiwan. $CHCl_3$ mole fractions in air are measured using a technique based on cryogenic pre-concentration and a capillary chromatograph–mass spectrometry (GC-MS)[35, 36]. The GSN station (33.3°N, 126.2°E) is situated on Jeju Island south of the Korean Peninsula, and mole fractions of $CHCl_3$ are measured using the Medusa GC-MS technology[37]. The time resolution of $CHCl_3$ measurements is every hour at HAT and every two hours at GSN. The HAT $CHCl_3$ measurements are reported

in NIES-11 calibration scale and in the SIO-98 calibration scale for GSN data. HAT $CHCl_3$ data were converted to the SIO-98 calibration scale using the NIES-11/SIO-98 ratio of 1.066+/-0.005.

Two inverse modeling techniques were used to resolve the regional emissions. One is a FLEXPART-based Bayesian inversion. Backward simulations from the FLEXPART model[14, 38] were driven by meteorological data (European Centre for Medium-Range Weather Forecasts - ECMWF). The backward simulations established a source–receptor relationship matrix, hereafter called "emission sensitivities". For computational efficiency, we assumed that source-receptor relationships for $CHCl_3$ were the same as for an unreactive gas. Our tests show that inferred East Asian total $CHCl_3$ emissions would change by only 1% if model runs that included $CHCl_3$ reactions with the OH radical were used. The FLEXPART model sensitivities were combined with a Bayesian optimization technique to derive the emission strengths in grid cells in East Asia. The cost function to be minimized is

$$J(x) = \frac{1}{2}(\boldsymbol{x} - \boldsymbol{x_a})^{\mathrm{T}}\mathbf{S}_a^{-1}(\boldsymbol{x} - \boldsymbol{x_a}) + \frac{1}{2}\left(\boldsymbol{y}^{\mathbf{obs}} - \mathbf{H}\boldsymbol{x_a}\right)^{\mathrm{T}}\mathbf{S}_{\mathrm{o}}^{-1}\left(\boldsymbol{y}^{\mathbf{obs}} - \mathbf{H}\boldsymbol{x_a}\right).$$

We find this minimum by solving $\nabla_x J(x) = 0$, which yields

$$\boldsymbol{x} = \boldsymbol{x_a} + \mathbf{S}_a\mathbf{H}^{\mathrm{T}}(\mathbf{H}\mathbf{S}_a\mathbf{H}^{\mathrm{T}} + \mathbf{S_o})^{-1}(\boldsymbol{y}^{\mathbf{obs}} - \mathbf{H}\boldsymbol{x_a}), \text{ and}$$

$$\mathbf{S}_b = (\mathbf{H}^{\mathrm{T}}\mathbf{S}_{\mathrm{o}}^{-1}\mathbf{H} + \mathbf{S}_a^{-1})^{-1}.$$

Here $\boldsymbol{x}$ is the state vector of emission strength ($g/m^2/s$) in each grid cell, $\boldsymbol{y}^{\mathbf{obs}}$ is $CHCl_3$ measurement vector, $\boldsymbol{x_a}$ is the prior emission vector, $\mathbf{H}$ is the emission sensitivity matrix derived from the FLEXPART backward simulation, $\mathbf{S}_a$ is the prior emission error covariance matrix, $\mathbf{S}_b$ is the posterior emission error covariance matrix, and $\mathbf{S_o}$ is the observational error covariance matrix. We set a uniform prior emission ($\boldsymbol{x_a}$) distribution over continents and oceans (Figure S5),

so that the posterior emissions are constrained from the measurement data. More information on constructing $\boldsymbol{x_a}$, $\mathbf{S}_a$ and $\mathbf{S_o}$ is provided in the Supplementary Information.

The second inversion method employed is a NAME-based hierarchical Bayesian inversion[16, 39]. NAME is the UK Met Office Lagrangian Particle Dispersion Model (LPDM), which was used here to simulate atmospheric transport. NAME was driven by meteorological information from the Met Office Unified Model, with spanned resolutions of 0.234°−0.563° (longitude) and 0.156°−0.375° (latitude) for 31−70 vertical levels over the period 2007−2015. NAME was run in backward-mode, for a maximum of 30 days backwards in time. For each observation, this resulted in sensitivity maps quantifying the relationship between surface (defined as 0-40 meters above ground level) emissions and concentrations at that receptor. The inversion using the NAME model used a hierarchical Bayesian methodology in which a set of "hyperparameters" comprising model-measurement uncertainties and prior emissions uncertainties were estimated simultaneously with fluxes. In addition, by employing a reversible jump trans-dimensional Markov chain Monte Carlo (TDMCMC) scheme, the spatial decomposition of the underlying flux field was also allowed to vary (i.e. the inversion grid over which fluxes are estimated), allowing the data to derive the resolution with which fluxes were inferred[39]. More information on NAME inversions is provided in the Supplementary Information.

Due to the emission sensitivity map coverage (Figure S6), emissions are only summed for a specific country/region within the domain between latitude: 20.8°N–44.0°N, 111.2°E– 146.0°E where our observations had significant sensitivity to potential sources.

Estimation of $CHCl_3$ impact on the recovery of Antarctic stratospheric ozone. Hossaini et al. constructed several scenarios showing the delay in ozone layer recovery (back to 1980 levels) due to various future elevated CH_2Cl_2 levels, compared to a reference scenario with zero

409 CH_2Cl_2[8]. They found that, to good approximation, Antarctic column ozone changes linearly with
410 the Cl_y load, and their simulations can be used to approximate the impact on ozone of other
411 chlorinated VSLSs of similar lifetime (the lifetime of CH_2Cl_2 and $CHCl_3$ are very similar, at 0.4
412 years[21]). Here, we make the further simplification that, for relatively small changes in column
413 ozone, the delay in ozone layer recovery can be scaled with Cl loading. Therefore, we use the
414 Hossaini et al. results to calculate the potential delay in ozone recovery due to $CHCl_3$ by scaling
415 their derived delay in proportion to increase in Cl loading due to $CHCl_3$ relative to CH_2Cl_2 in
416 2050. We explore a "continued growth" scenario that the atmospheric $CHCl_3$ mole fraction
417 grows at 2010−2015 rates. In 2015, the mole fraction of $CHCl_3$ was ~15 pmol mol^{-1} in the
418 Northern Hemisphere, as presented Figure 1b, and would reach ~40 pmol mol^{-1} in 2050. To
419 investigate the impact of only the recent rise in $CHCl_3$ emissions, 2010 mole fractions (~12 pmol
420 mol^{-1} in the Northern Hemisphere as presented in Figure 1b) are subtracted. In Scenario 1 in the
421 Hossaini et al. paper, the mole fraction of CH_2Cl_2 in the Northern Hemisphere was ~60 pmol
422 mol^{-1} and would reach ~165 pmol mol^{-1} in 2050[8]. This scenario in Hossaini showed a delay in
423 ozone recovery between 30 years (based on chemical transport model simulations) and 17 years
424 (based on chemistry-climate model simulations). Thus, the Antarctic stratospheric ozone
425 recovery could be delayed due to continuous growth of $CHCl_3$ by approximately 4 (17x(40-
426 12)/165x(3/2)) and 8 (30x(40-12)/165x(3/2)) years (the factor of 3/2 is because $CHCl_3$ has three
427 Cl atoms per molecule and CH_2Cl_2 has two). Whilst $CHCl_3$ demand and production in China is
428 projected to increase in near-term[29] (see details in SI), future emissions trends are of course
429 highly uncertain. Therefore, we present an alternative scenario ("constant mole fraction"), which
430 assumes that future $CHCl_3$ mole fractions will remain at the level of ~15 pmol mol^{-1}, as observed
431 in 2015. The corresponding Scenario 3 (no future growth of CH_2Cl_2 mole fractions of ~60 pmol

mol^{-1} through 2050) in Hossaini et al. showed a 5-year delay in recovery compared to their baseline scenario. Thus, the ozone layer recovery delay in this "constant 2015 mole fraction" scenario for $CHCl_3$ is about 0.4 (5x(15-12)/60x3/2 =0.4) years. In addition to the assumptions described above, these calculations are thought to be weakly sensitive to differences in the lifetime and atmospheric distribution of $CHCl_3$ and CH_2Cl_2. Furthermore, they rely on simulations from only the two models used in Hossaini et al.

Data availability. The data that support the findings of this study are available from the corresponding author upon request. $CHCl_3$ measurement data for East Asia can be accessed by contacting data leads: S.P. (sparky@knu.ac.kr) for GSN and T.S. (saito.takuya@nies.go.jp) for HAT. $CHCl_3$ measurement data for the five non-Asian AGAGE stations (CGO, SMO, RPB, THD, MHD) used in this study are available at http://agage.mit.edu/data/agage-data/.

Code availability. Code for the AGAGE 2-D atmospheric 12-box model and inversion is available upon request from M.R.. Code for the Lagrangian particle transport model (FLEXPART) is available at https://www.flexpart.eu/. Code for the UK Met Office's Numerical Atmospheric-dispersion Modelling Environment model (NAME) is available at https://www.metoffice.gov.uk/research/modelling-systems/dispersion-model or upon request from A.J.M.. Code for the FLEXPART-based Bayesian inversion is available upon request from X.F.. Code for the NAME-based hierarchical Bayesian inversion is available upon request from M.R. and A.L.G..

References for Methods

30. Rigby, M., *et al.* Re-evaluation of the lifetimes of the major CFCs and CH3CCl3 using atmospheric trends. *Atmos. Chem. Phys.* **13,** 2691-2702 (2013).

31. Cunnold, D. M.*, et al.* The Atmospheric Lifetime Experiment: 3. Lifetime methodology and application to three years of CFCl3 data. *J. Geophys. Res. Oceans* **88,** 8379-8400 (1983).

32. Rigby, M., Ganesan, A. L., Prinn, R. G. Deriving emissions time series from sparse atmospheric mole fractions. *J. Geophys. Res. Atmos.* **116,** 306-310 (2011).

33. Xiao, X. Optimal Estimation of the Surface Fluxes of Chloromethanes Using a 3-D Global Atmospheric Chemical Transport Model. Ph.D. thesis, Massachusetts Institute of Technology, 2008.

34. Rigby, M.*, et al.* Recent and future trends in synthetic greenhouse gas radiative forcing. *Geophys. Res. Lett.* **41,** 2623-2630 (2014).

35. Enomoto, T., Yokouchi, Y., Izumi, K., Inagaki, T. Development of an analytical method for atmospheric halocarbons and its application to airborne observation (in Japanese). *J. Jpn. Soc. Atmos. Environ.* **40,** 1-8 (2005).

36. Yokouchi, Y.*, et al.* High frequency measurements of HFCs at a remote site in east Asia and their implications for Chinese emissions. *Geophys. Res. Lett.* **33,** 814-817 (2006).

37. Miller, B. R.*, et al.* Medusa: A sample preconcentration and GC/MS detector system for in situ measurements of atmospheric trace halocarbons, hydrocarbons, and sulfur compounds. *Anal. Chem.* **80,** 1536-1545 (2008).

38. Stohl, A., Forster, C., Frank, A., Seibert, P., Wotawa, G. Technical note: The Lagrangian particle dispersion model FLEXPART version 6.2. *Atmos. Chem. Phys.* **5,** 2461-2474 (2005).

39. Lunt, M. F., Rigby, M., Ganesan, A. L., Manning, A. J. Estimation of trace gas fluxes with objectively determined basis functions using reversible-jump Markov chain Monte Carlo. *Geosci. Model Dev.* **9,** 3213-3229 (2016).

Supplementary Information

Rapid increase in ozone-depleting chloroform emissions from China

Xuekun Fang[1*], Sunyoung Park[2], Takuya Saito[3], Rachel Tunnicliffe[4,5], Anita L. Ganesan[5*], Matthew Rigby[4*], Shanlan Li[2], Yoko Yokouchi[3], Paul J. Fraser[6], Christina M. Harth[7], Paul B. Krummel[6], Jens Mühle[7], Simon O'Doherty[4], Peter K. Salameh[6], Peter G. Simmonds[4], Ray F. Weiss[7], Dickon Young[4], Mark F. Lunt[4], Alistair J. Manning[8], Alicia Gressent[1], Ronald G. Prinn[1]

[1]Center for Global Change Science, Massachusetts Institute of Technology, Cambridge, Massachusetts, USA

[2]Department of Oceanography, Kyungpook National University, Daegu, South Korea

[3]National Institute for Environmental Studies, Tsukuba, Japan

[4]School of Chemistry, University of Bristol, Bristol, UK

[5]**School of Geographical Sciences, University of Bristol, Bristol, UK**

[6]Climate Science Centre, CSIRO Oceans and Atmosphere, Aspendale, Victoria, Australia

[7]Scripps Institution of Oceanography, University of California, San Diego, La Jolla, California, USA

[8]Met Office, Exeter, United Kingdom

*e-mail: fangxk@mit.edu (X.F.); anita.ganesan@bristol.ac.uk (A.L.G.); matt.rigby@bristol.ac.uk (M.R.)

Global $CHCl_3$ emission estimation

Global emissions were calculated using baseline atmospheric data from five remote AGAGE stations (MHD, THD, RPB, SMO, CGO). Baseline monthly means were estimated by statistically filtering the high-frequency data, as described by O'Doherty et al.[1]. The data were averaged into semi-hemispheres (30°N–90°N, 0°N–30°N, 30°S–0°S, 90°S–30°S) for comparison with mole fractions predicted by the AGAGE 12-box model, which resolves four semi-hemispheres, with vertical levels separated at 500 and 200 hPa[2, 3]. The model uses annually repeating meteorology and OH concentrations from Spivakovsky et al.[4], tuned to match the growth rate of methyl chloroform. A temperature dependent rate constant for the reaction of $CHCl_3$ with tropospheric OH from Burkholder et al.[5] was used, leading to a lifetime in the model of 0.6 years. A Bayesian framework was used to derive emissions from the data and the model, in which prior estimate of the emissions growth rate was adjusted to bring the model into agreement with the data (following Rigby et al.[6]). For this work, our prior estimate was assumed to be zero emissions growth from one year to the next, with a 1-sigma uncertainty in this assumption somewhat arbitrarily chosen to be 20% of the Xiao et al. bottom-up emissions estimate[7]. The inversion propagates uncertainties in the observations through to the derived fluxes, and augments the derived fluxes with uncertainties due to the lifetime and potential errors in the calibration scale[8].

FLEXPART-based regional emission inversion

In the FLEXPART-based inversion, a Bayesian inversion technique was used. See the equations in main text. $\boldsymbol{x_a}$ is the prior emission vector. There is no gridded emission inventory available for

525 $CHCl_3$. Thus, we used a spatially and temporally uniform prior distribution across the land and
526 ocean domains. The prior total East Asian $CHCl_3$ emissions from land were set to the amount
527 estimated by Li et al.[9] (49.5 Gg yr^{-1}). The prior total emissions from the ocean were set to 168
528 Gg yr^{-1}, according to estimates by Xiao et al.[7]. The map of prior emissions is shown in Figure S5.
529 Prior emissions were the same for all years during 2007−2015. Variable-resolution emission grid
530 boxes were used in the inversions. Following the allocation method by Stohl et al.[10], grid sizes
531 ranged from 24°×24° to 1°×1°, with fine resolution in regions with high emission sensitivity and
532 emission strength (e.g., Eastern China. South Korea, and Japan) and coarse resolutions in remote
533 regions (e.g., Western China and ocean). $\mathbf{S}_a$ is the prior emission error covariance matrix. There
534 is no knowledge of prior emissions and their uncertainties. Here we set the prior emission
535 uncertainty to be 500% of the emission in each grid box, squared values of which are the
536 diagonal elements of $\mathbf{S}_a$.

537 The 2-hourly (GSN) and hourly (HAT) $CHCl_3$ measurement data were averaged into daily
538 means and then assimilated in the inversions. The observational error covariance matrix $\mathbf{S}_o$ was
539 equal to the sum of $\mathbf{S}_{observation}$ and $\mathbf{S}_{emis\_aggregation}$[11, 12, 13]

540 $$\mathbf{S}_o = \mathbf{S}_{observation} + \mathbf{S}_{emis\_aggregation}$$

541 The diagonal elements of $\mathbf{S}_{observation}$ are squared $\sigma_{observation}$. Calculation of $\sigma_{observation}$ is as
542 follows

543 $$\sigma_{observation} = \sqrt{\sigma^2_{obs\_precision} + \sigma^2_{obs\_representation} + \sigma^2_{obs\_intercalibration} + \sigma^2_{background}}.$$

544 Here $\sigma_{obs\_precision}$ is the precision of $CHCl_3$ measurement (1% and 1% were used for HAT and
545 GSN stations, respectively), $\sigma_{obs\_representation}$ is the uncertainty of how representative the

observations are and we used one-sigma standard deviation of the observations that were averaged for each daily value, $\sigma_{obs\_intercalibration}$ is 0.005/1.066=0.47% for HAT station (NIES-11/SIO-98 ratio of 1.066+/-0.005), $\sigma_{\mathrm{background}}$ is the variation of background defined by different methodologies or setups (the mole fraction background filtering method for the FLEXPART inversion is the same as described in detail by Stohl et al.[10]; here, we used various setups in its calculation, e.g., 5 days or 8 days window to calculate the $\sigma_{\mathrm{background}}$). The observation errors $\sigma_{observation}$ were assumed to be uncorrelated, since the measurement data used in FLEXPART inversions were daily averages. Consequently $\mathbf{S}_{observation}$ only has diagonal elements.

$\mathbf{S}_{emis\_aggregation}$ is the aggregation error from aggregating the spatial emissions from fine grid cell resolution to variable resolution grid. Calculation of $\mathbf{S}_{emis\_aggregation}$ follows the method of Kaminski et al.[11] and Thompson et al.[12]:

$$\mathbf{S}_{emis\_aggregation} = \mathbf{HPS}_{a\_fine}\mathbf{P}^{\mathrm{T}}\mathbf{H}^{\mathrm{T}}$$

where $\mathbf{S}_{a\_fine}$ is the prior emission error covariance matrix at fine grid cell resolution (while $\mathbf{S}_a$ is the prior emission error covariance matrix at variable-resolution grid). $\mathbf{P}$ represents the projection of the loss of information in the variable resolution grid compared to the fine grid, which can be calculated following the equations in Thompson et al.[12]. Since $\mathbf{S}_{emis\_aggregation}$ has off-diagonal elements, $\mathbf{S}_{\boldsymbol{o}}$ (sum of $\mathbf{S}_{observation}$ and $\mathbf{S}_{emis\_aggregation}$) also has off-diagonal elements.

NAME-based regional emission inversion

Where possible, the set up for the NAME-based inversion was matched to the FLEXPART inversion method, including use of the same prior emissions field. Here, we describe differences between the NAME and FLEXPART inversion methodologies. In the NAME-TDMCMC inversion, the spatial grid (i.e. the number and placement of resolved regions) over which the flux field was estimated was allowed to vary within a sub-domain (20.8°N–44.0°N, 111.2°E–146.0°E). Surrounding this sub-domain, emissions were inferred for eight fixed regions, which were not spatially varying. The inversion domain thus spanned 5.2°S–74.1°N, 54.5°E–191.8°E) but results are only presented for the inner sub-domain. Outside of this inversion domain, boundary conditions were estimated as adjustments to vertically uniform 'curtains' on each edge of the inversion domain. Prior values for these curtains were mole fraction baseline data for $CHCl_3$, calculated using the AGAGE 12-box model from 1997–2016 within latitude bands of 90°N–30°N, 30°N–0°N, 0°S–30°S and 30°S–90°S[2, 3]. The mean value was used across each latitude band. Though no measurement site within the East Asian domain of this study was used for the model, the stations which were used are positioned to allow good coverage within each semi-hemisphere. By tracking the location of particles exiting the inversion domain, boundary conditions were mapped to these curtains. Adjustments to the boundary conditions were made in the inversion by solving for a scaling to each of these curtains simultaneously with other parameters. $CHCl_3$ measurement data at HAT and GSN stations were averaged over 24 hours and inversions were run for one year at a time. Prior to averaging, the data were filtered to reduce the contribution of local influence (i.e. unresolved emissions). Using the NAME sensitivity maps, for each measurement, a ratio was determined between the sensitivity local to the station (within 0.47° latitude 0.70° longitude; equivalent to two grid cells) and the total across the

domain. If this local ratio was greater than 10%, the associated measurement point at that time was removed, implying that air was likely stagnant and more prone to local unresolved sources. While fluxes and hyper-parameters (model-measurement uncertainties, prior uncertainties, correlation timescales) were estimated with annual resolution, boundary conditions were estimated on a monthly basis to allow for seasonal variation. Lognormal probability density functions (PDF) used to describe fluxes and boundary conditions and uniform PDFs were used for hyper-parameters. For each inversion, the parameters and hyper-parameters were sampled 100,000 times with an additional 100,000 burn-in iterations, storing every 100th sample for analysis. The simulated $CHCl_3$ mole fractions are shown alongside observed values for these inversions in Figure S2.

$CHCl_3$ historical and future demand in China

In China, $CHCl_3$ is widely used for producing polytetrafluoroethylene (PTFE). The chemical reaction equations for producing PTFE using $CHCl_3$ are shown below. The capacity of PTFE production increased at 11%/yr between 2010 and 2015, and was projected to increase at 5.3%/yr between 2015 and 2020[14]. The PTFE production increased at 17%/yr between 2010 and 2015, and was projected to increase at 7%/yr between 2015 and 2020 (almost a linear increase between 2010 and 2020)[14]. Industrial reports of $CHCl_3$ annual production are currently unavailable. Therefore, PTFE production data in the past (2010–2015) and projected 2015–2020 periods indicates an increasing demand for and production of $CHCl_3$ in these two periods.

$$CaF_2 + H_2SO_4 \rightarrow 2HF + CaSO_4 \qquad (1)$$

$$CHCl_3(\text{chloroform}) + 2HF \rightarrow CHClF_2 + 2HCl \qquad (2)$$

$$2CHClF_2 \rightarrow CF_2 = CF_2 + 2HCl \qquad (3)$$

$$nCF_2 = CF_2 \rightarrow -(F_2C - CF_2)_n - \qquad (4)$$

References

1. O'Doherty, S.*, et al.* In situ chloroform measurements at Advanced Global Atmospheric Gases Experiment atmospheric research stations from 1994 to 1998. *J. Geophys. Res. Atmos.* **106,** 20429-20444 (2001).

2. Cunnold, D. M.*, et al.* The Atmospheric Lifetime Experiment: 3. Lifetime methodology and application to three years of CFCl3 data. *J. Geophys. Res. Oceans* **88,** 8379-8400 (1983).

3. Rigby, M.*, et al.* Re-evaluation of the lifetimes of the major CFCs and CH3CCl3 using atmospheric trends. *Atmos. Chem. Phys.* **13,** 2691-2702 (2013).

4. Spivakovsky, C. M.*, et al.* Three-dimensional climatological distribution of tropospheric OH: Update and evaluation. *J. Geophys. Res. Atmos.* **105,** 8931-8980 (2000).

5. Burkholder, J. B., Sander, S. P., Abbatt, J. P. D., Barker, J. R., Huie, R. E., Kolb, C. E., Kurylo, M. J., Orkin, V. L., Wilmouth, D. M. and Wine, P. H *Chemical Kinetics and Photochemical Data for Use in Atmospheric Studies, Evaluation No. 18* (2015)

6. Rigby, M., Manning, A. J., Prinn, R. G. Inversion of long-lived trace gas emissions using combined Eulerian and Lagrangian chemical transport models. *Atmos. Chem. Phys.* **11,** 9887-9898 (2011).

7. Xiao, X. Optimal Estimation of the Surface Fluxes of Chloromethanes Using a 3-D Global Atmospheric Chemical Transport Model. Ph.D. thesis, Massachusetts Institute of Technology, 2008.

8. Rigby, M.*, et al.* Recent and future trends in synthetic greenhouse gas radiative forcing. *Geophys. Res. Lett.* **41,** 2623-2630 (2014).

9. Li, S.*, et al.* Emissions of Halogenated Compounds in East Asia Determined from Measurements at Jeju Island, Korea. *Environ. Sci. Technol.* **45,** 5668-5675 (2011).

10. Stohl, A.*, et al.* An analytical inversion method for determining regional and global emissions of greenhouse gases: Sensitivity studies and application to halocarbons. *Atmos. Chem. Phys.* **9,** 1597-1620 (2009).

11. Kaminski, T., Rayner, P. J., Heimann, M., Enting, I. G. On aggregation errors in atmospheric transport inversions. *J. Geophys. Res. Atmos.* **106,** 4703-4715 (2001).

12. Thompson, R. L., Stohl, A. FLEXINVERT: an atmospheric Bayesian inversion framework for determining surface fluxes of trace species using an optimized grid. *Geosci. Model Dev.* **7,** 2223-2242 (2014).

13. Trampert, J., Snieder, R. Model Estimations Biased by Truncated Expansions: Possible Artifacts in Seismic Tomography. *Science* **271,** 1257-1260 (1996).

14. Qianzhan. China's fluoropolymer production capacity will be 230,000 tons by 2020, and PTFE will account for 70% (in Chinese). 2017. Available from: https://www.qianzhan.com/analyst/detail/220/170629-c33a2ca7.html

15. Chinairn. Price of feedstock for CHCl3 goes up and demand for CHCl3 grows (in Chinese). 2014. Available from: http://www.chinairn.com/news/20140512/164033296.shtml

16. Yan, C.*, et al.* Analysis on market prospects of chlorinated methanes in China (in Chinese with English abstract). *Chlor-Alkali Industry* **45,** 1-4 (2009).

Tables

Table S1. The distance (pmol mol^{-1}) of 90th percentile and 10th percentile of $CHCl_3$ mole fractions at each station (an approximation of the pollution magnitude) and the corresponding change rates (pmol mol^{-1} yr^{-1}; using the "least squares" method; the range represents the regression coefficients±standard error) over 2007−2015. The change rates for MHD, THD, RPB, SMO and CGO stations are very close to zero, which suggests regional $CHCl_3$ emissions in Australia (based on CGO station), North America (THD station) and Europe (MHD station) likely did not increase. Change rates for GSN and HAT stations in East Asia are tens and hundreds times larger, which suggests rapid changes in $CHCl_3$ emissions in East Asia. Subsequently, FLEXPART-based and NAME-based inversions are used to quantify the East Asian $CHCl_3$ emissions.

	MHD	THD	RPB	SMO	CGO	GSN	HAT
2007	9.6	4.6	2.3	1.7	8.8	16.8	12.0
2008	8.6	5.8	2.8	1.5	8.5	21.9	13.3
2009	7.3	5.3	2.4	1.5	8.2	19.8	15.5
2010	8.6	4.7	2.0	1.7	7.9	25.1	16.3
2011	7.2	4.9	3.0	1.4	8.2	21.3	15.5
2012	7.9	4.9	2.9	1.5	7.8	18.5	18.7
2013	8.4	6.4	3.4	1.5	7.8	34.7	22.8
2014	10.1	6.2	2.9	1.7	9.4	36.8	27.4
2015	9.3	6.0	3.1	1.7	9.6	56.4	27.9
Change rate over 2007−2015	-0.06−0.21	0.07−0.22	0.07−0.15	-0.01−0.02	-0.01−0.17	2.73−4.80	1.80−2.30

Table S2. $CHCl_3$ emissions (Gg/yr) from each East Asian country/region and the globe.

		2007	2008	2009	2010	2011	2012	2013	2014	2015
FLEXPART inversion	Eastern China	32 (26−38)	39 (34−45)	30 (25−36)	39 (34−45)	36 (30−42)	42 (36−49)	48 (42−53)	60 (55−65)	88 (80−95)
	Taiwan	1.0 (0.1−1.9)	0.2 (0.0−0.7)	1.5 (0.7−2.2)	0.3 (0.0−1.0)	0.3 (0.0−0.8)	1.1 (0.4−1.9)	0.3 (0.0−0.9)	0.3 (0.0−0.7)	1.4 (0.6−2.2)
	North Korea	0.4 (0.0−1.3)	0.8 (0.0−1.8)	0.3 (0.0−1.0)	0.9 (0.0−2.0)	0.3 (0.0−0.9)	0.8 (0.0−1.9)	1.1 (0.1−2.1)	0.7 (0.0−1.6)	0.9 (0.0−1.9)
	South Korea	1.3 (0.3−2.3)	2.2 (1.4−3.0)	2.1 (1.3−3.0)	0.9 (0.2−1.7)	1.9 (1.1−2.8)	1.4 (0.6−2.2)	1.1 (0.4−1.8)	0.7 (0.1−1.4)	2.9 (2.0−3.9)
	Japan	4.7 (1.8−7.6)	4.4 (1.8−7.1)	4.7 (2.3−7.1)	3.6 (0.6−6.5)	3.6 (1.1−6.1)	2.3 (0.1−4.4)	4.0 (1.6−6.4)	6.1 (3.7−8.5)	2.2 (0.2−4.2)
NAME inversion	Eastern China	51 (45−57)	49 (43−54)	40 (35−44)	32 (26−40)	55 (49−62)	51 (38−64)	63 (56−69)	81 (72−90)	82 (70−101)
	Taiwan	1.2 (0.4−2.2)	0.3 (0.0−0.6)	0.6 (0.2−1.2)	0.2 (0.0−0.3)	0.3 (0.1−0.8)	0.3 (0.0−0.6)	0.4 (0.0−1.0)	0.6 (0.0−1.6)	0.7 (0.2−1.6)
	North Korea	0.9 (0.2−2.1)	0.9 (0.4−1.7)	0.9 (0.3−1.8)	0.3 (0.0−0.9)	1.5 (0.6−2.6)	1.0 (0.1−2.2)	1.1 (0.4−2.4)	1.6 (0.7−2.6)	2.6 (1.1−4.3)
	South Korea	1.0 (0.3−1.7)	1.4 (0.8−2.1)	2.0 (1.5−2.6)	2.1 (1.7−2.5)	1.8 (1.4−2.4)	1.8 (1.3−2.3)	1.2 (0.4−2.2)	2.0 (1.4−2.7)	2.1 (0.9−3.7)
	Japan	5.1 (1.7−8.5)	5.2 (3.0−7.9)	4.0 (1.8−6.0)	1.9 (0.4−4.6)	11.8 (7.7−16.6)	2.8 (0.7−4.8)	1.3 (0.2−2.9)	8.6 (5.0−12.4)	7.5 (3.7−10.9)
AGAGE 12-box inversion	Globe	277 (222−340)	272 (219−332)	259 (209−320)	279 (227−341)	279 (222−340)	290 (234−356)	306 (247−373)	321 (256−392)	324 (261−397)

Table S3. Location information of major $CHCl_3$ factories in China[15, 16] (may not be complete; latitude/longitude information was obtained by using google earth).

Factory number	Latitude	Longitude
1	37.0	118.5
2	31.7	121.0
3	29.3	104.8
4	37.1	119.0
5	37.0	118.0
6	32.5	119.9
7	36.4	116.2
8	28.9	118.9
9	32.2	119.6

Table S4. Information of *in situ* $CHCl_3$ measurement sites used in this study.

Station	Code	Latitude	Longitude	Altitude (m a.s.l.)	Calibration scale
Mace Head, Ireland	MHD	53.3°N	9.9°W	5	SIO-98
Trinidad Head, California, USA	THD	41.1°N	124.2°W	107	SIO-98
Ragged Point, Barbados	RPB	13.2°N	59.4°W	45	SIO-98
Cape Matatula, American Samoa	SMO	14.2°S	170.6°W	77	SIO-98
Cape Grim, Tasmania, Australia	CGO	40.7°S	144.7°E	94	SIO-98
Gosan, South Korea	GSN	33.3°N	126.2°E	72	SIO-98
Hateruma, Japan	HAT	24.1°N	123.8°E	47	NIES-11

Table S5. Performance of FLEXPART and NAME inversions on simulating $CHCl_3$ mole fractions at HAT and GSN stations. $\boldsymbol{B}$ represents the mean bias (pmol mol^{-1}) between the simulations and measurements (simulated values minus measurements). $\boldsymbol{r}$ represents Pearson correlation coefficients between the simulations and measurements. $\boldsymbol{RMSE}$ represents the root mean square error (pmol mol^{-1}) between the simulations and measurements.

Station	Year	$\boldsymbol{B}$		$\boldsymbol{r}$		$\boldsymbol{RMSE}$	
		FLEXPART inversion	NAME inversion	FLEXPART inversion	NAME inversion	FLEXPART inversion	NAME inversion
HAT	2007	-0.73	1.37	0.80	0.81	3.42	3.81
	2008	-0.52	0.91	0.84	0.85	3.07	3.35
	2009	-0.84	-0.07	0.80	0.89	3.28	3.01
	2010	-0.29	0.66	0.89	0.84	3.54	4.31
	2011	-0.99	0.55	0.84	0.91	3.98	3.09
	2012	-0.93	1.35	0.90	0.89	3.88	4.35
	2013	-2.13	0.06	0.90	0.89	5.21	4.95
	2014	-0.80	0.46	0.93	0.88	4.05	5.58
	2015	-0.14	0.89	0.92	0.84	4.12	6.36
GSN	2007	-0.90	-1.32	0.68	0.84	4.94	4.25
	2008	-0.87	-1.58	0.83	0.82	5.17	5.64
	2009	-2.02	-1.10	0.69	0.83	6.77	6.17
	2010	-2.08	-1.62	0.89	0.82	7.31	6.49
	2011	-1.11	1.00	0.75	0.63	5.17	8.37
	2012	-1.79	0.50	0.78	0.85	5.99	5.03
	2013	-3.93	-3.86	0.79	0.75	11.40	10.73
	2014	-3.06	-1.00	0.79	0.85	10.64	8.20
	2015	-6.22	-8.34	0.80	0.73	17.41	22.83

Figures

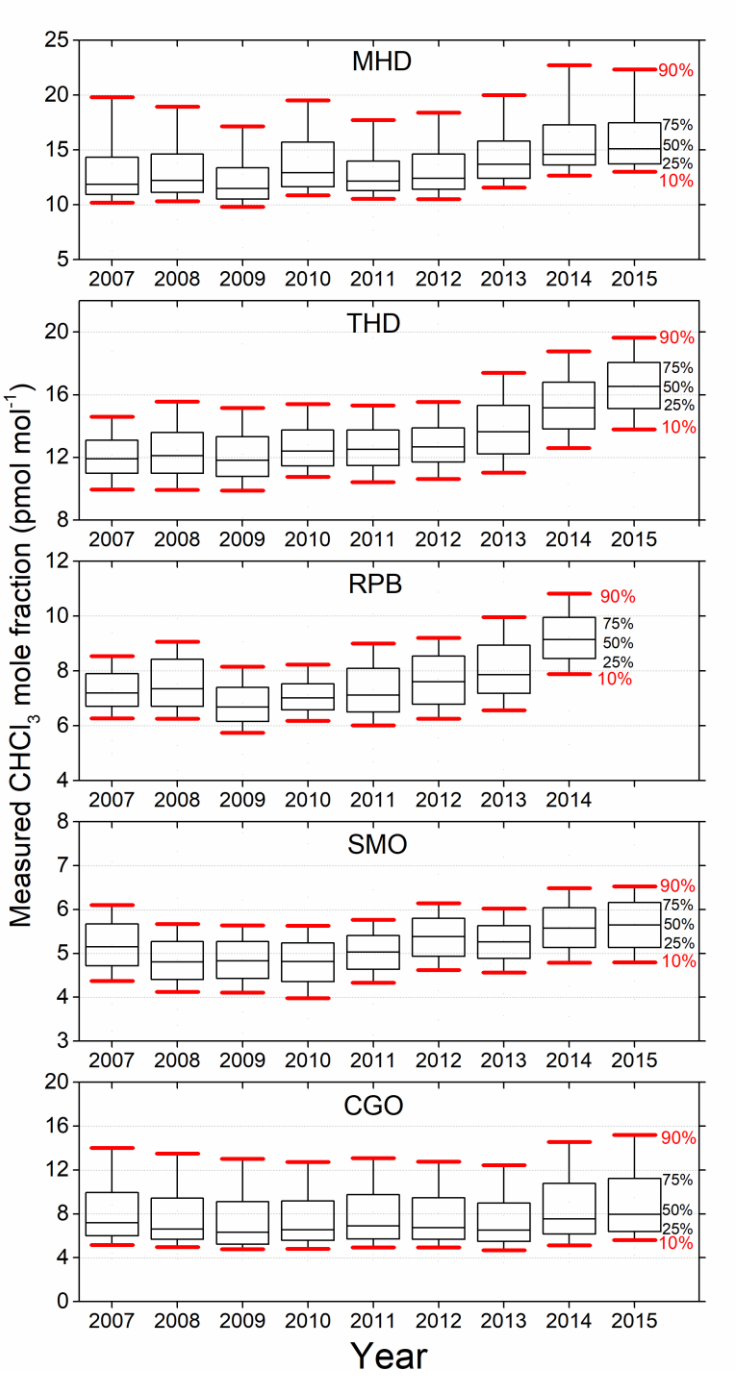

Figure S1. Box and whisker plots for the measured $CHCl_3$ mole fractions at MHD, THD, RPB, SMO and CGO stations. The 10^{th}, 25^{th}, 50^{th}, 75^{th} and 90^{th} percentiles are shown. The distance of 90^{th} percentile and 10^{th} percentile is an approximation of the pollution magnitude and is related to the regional emission strength of $CHCl_3$. RPB data for 2015 are not included due to biased low CHCl3 mole fraction values induced by no measurements in some months in 2015. Statistics of enhanced $CHCl_3$ mole fractions for each station, as well as GSN and HAT stations, are provided in Table S1.

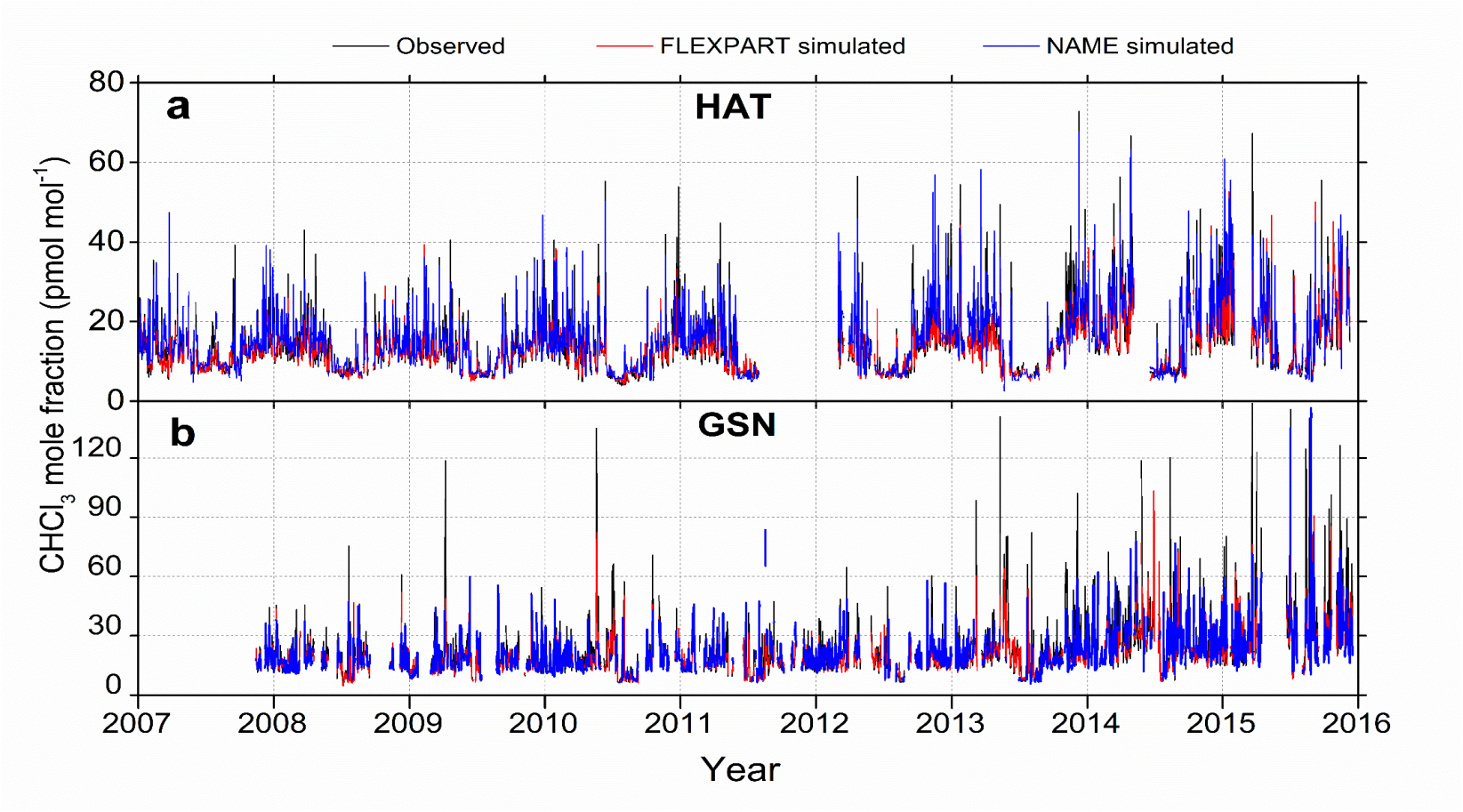

Figure S2. Observed and simulated $CHCl_3$ mole fractions at HAT and GSN stations from FLEXPART and NAME inversions. Statistics of performance of FLEXPART and NAME inversions on simulating $CHCl_3$ mole fractions for each station are provided in Table S5. Note that some measurement points were excluded by a filter algorithm in NAME inversions (see main text).

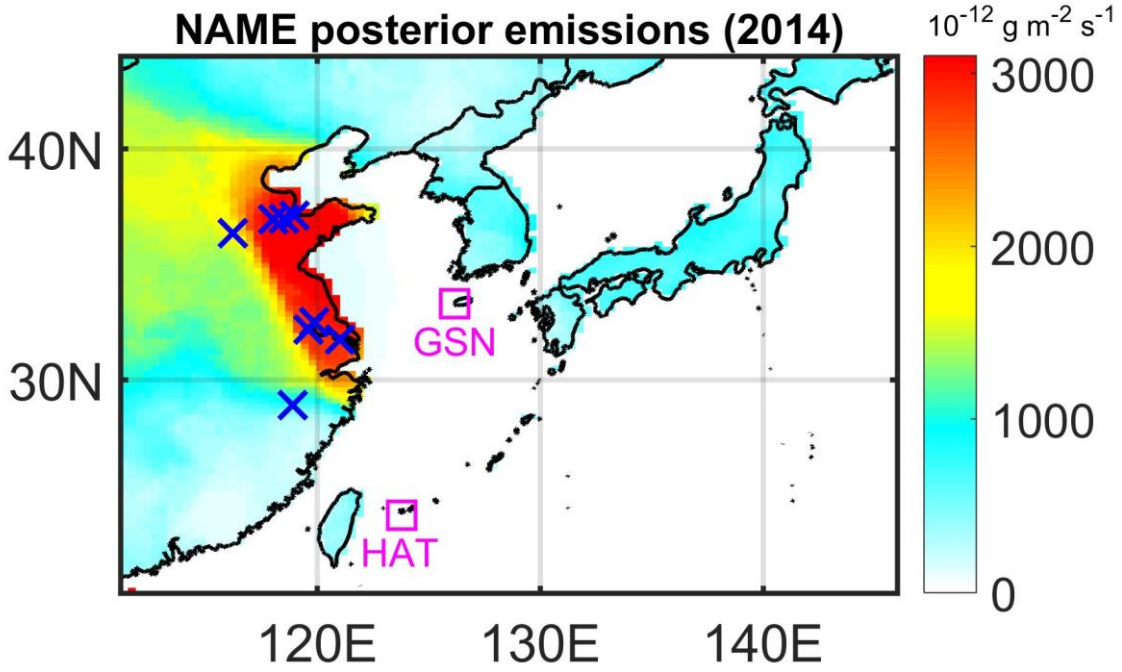

Figure S3. Map of posterior $CHCl_3$ emissions derived from NAME inversion. The blue crosses represent the factories of $CHCl_3$ production and the purple squares represent the measurement stations.

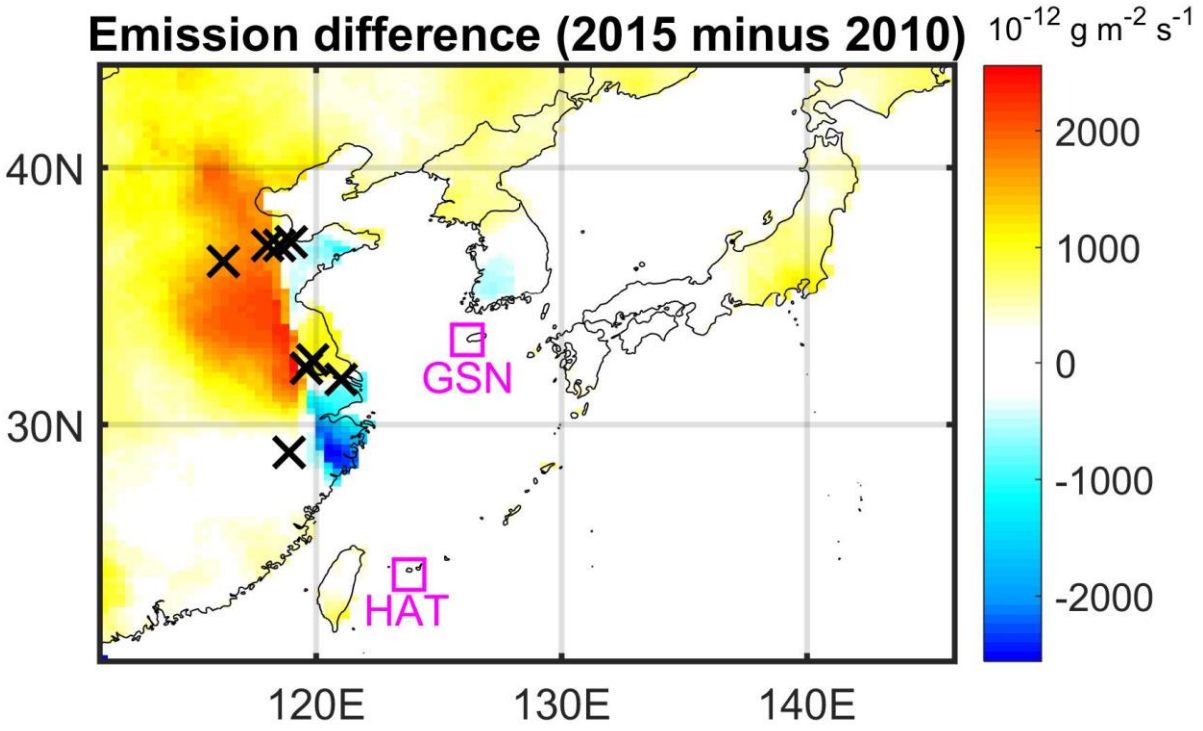

Figure S4. Spatial differences of posterior emissions between 2015 and 2010 (2015 minus 2010; NAME-based inversions). The black crosses represent the factories of $CHCl_3$ production and the purple squares represent the measurement stations.

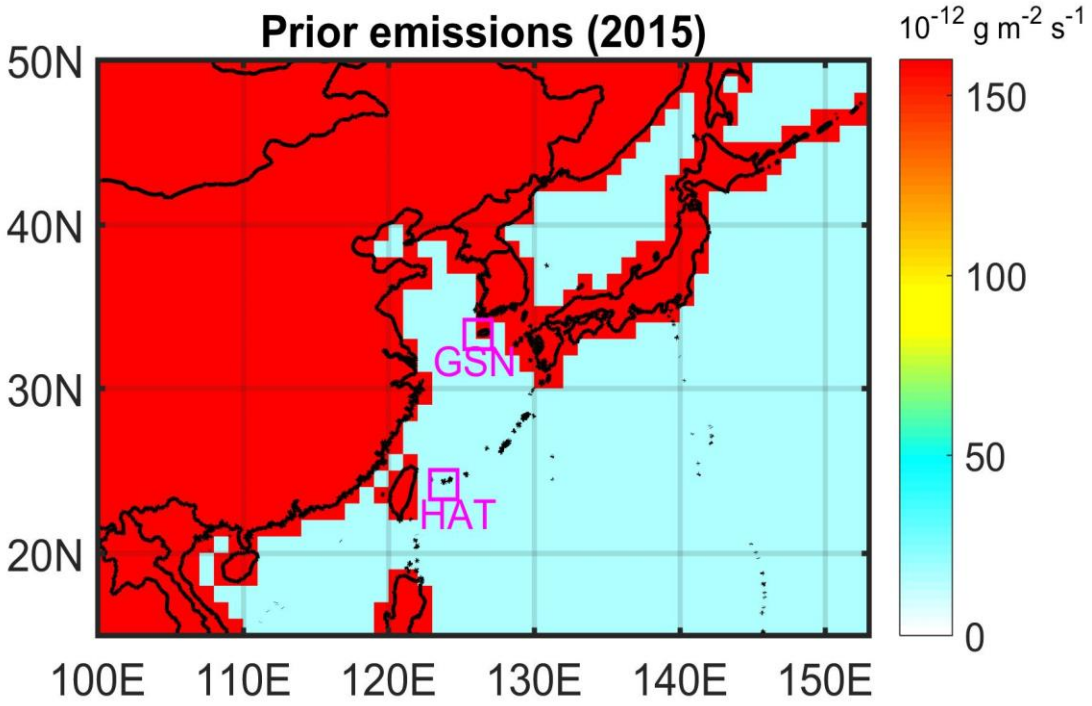

Figure S5. Map of prior $CHCl_3$ emissions from continent and ocean used in FLEXPART and NAME inversions. Prior emissions are the same for all years during 2007−2015.

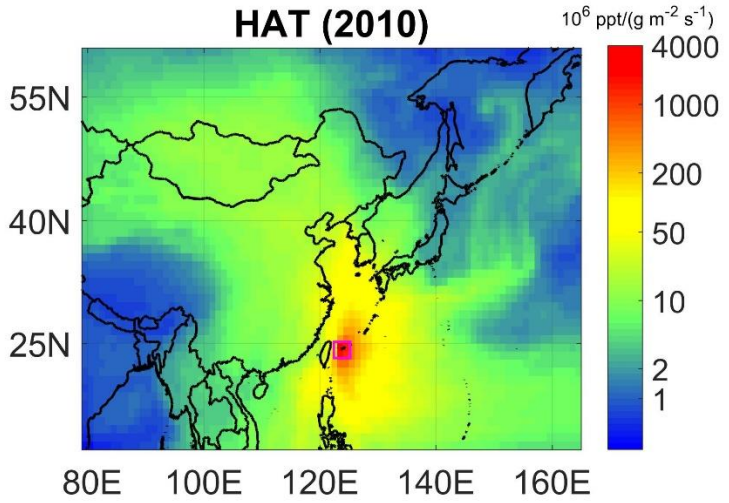

716

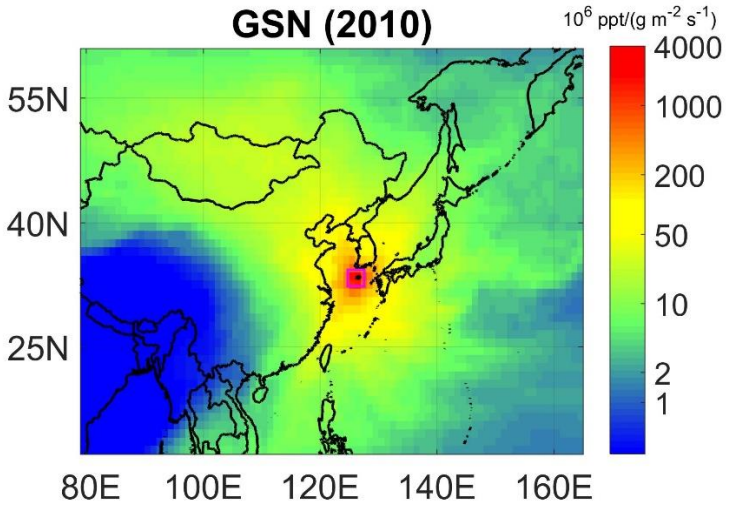

717

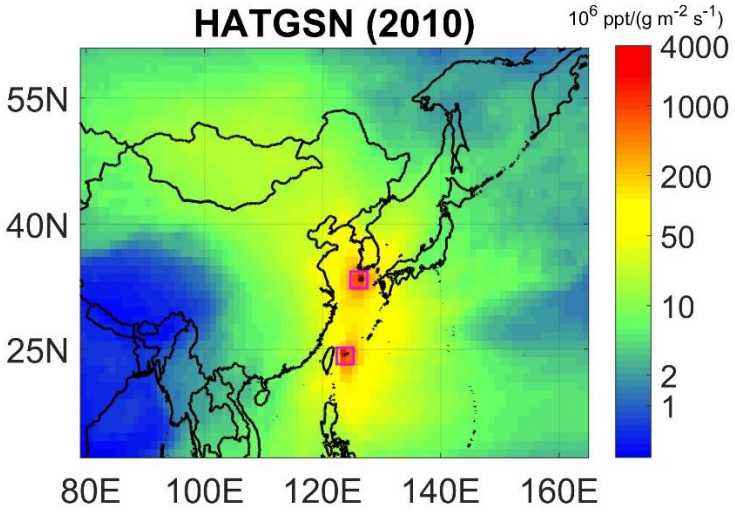

718

719 **Figure S6. Annual average emission sensitivity from FLEXPART simulations for HAT, GSN**
720 **and HATGSN stations for the year 2010.** The purple squares represent the measurement stations.

721